

## Distribution of Excitation Transfer in Helium\*

John D. Jobe<sup>†</sup> and Robert M. St. John

*Department of Physics and Astronomy, University of Oklahoma, Norman, Oklahoma 73069*

(Received 21 June 1971)

The distribution of atom-atom collisional excitation among various levels of the helium atom is determined. The determination is made by analyzing absolute measurements of the optical electron excitation cross sections of 63 levels at 100 eV electron energy and 63 mTorr pressure. Factors pertaining to our method of obtaining absolute optical cross sections are discussed in some detail. Collisional-excitation transfer on the  $n=3$  level is found to be slight with a cross section for  $3^1P$  to  $3^1D$  transfer of less than  $1.2 \times 10^{-15} \text{ cm}^2$ . A detailed analysis is made on the  $n=4$  level and collisional excitation transfer cross sections are found to be  $(4.7 \pm 1.5) \times 10^{-14} \text{ cm}^2$  for  $4F$  to  $4D$  transfer and  $(2.3 \pm 0.6) \times 10^{-14} \text{ cm}^2$  for  $4^1P$  to  $4F$  transfer. The pressure dependence of the apparent electron excitation cross sections of 47 levels is also presented at 100 eV electron energy. Our work shows that the apparent cross sections of levels with large principal quantum numbers decrease as the pressure increases, an effect opposite to that observed for levels of low principal quantum number. A short discussion explains these phenomena in terms of a cyclic energy-exchange process which includes electron excitation, imprisonment of resonance radiation, collisional excitation transfer, and radiative transfer. In the course of this investigation it was necessary to obtain values for the electron excitation cross sections of the  $n^1P$  series up to  $n=10$ . The values showed good agreement with Born-approximation theoretical cross sections.

### I. INTRODUCTION

This work was undertaken in order to clarify the processes which cause the apparent electron excitation cross sections of helium to show marked dependence upon the ground-state density. The present study is based on absolute measurements of apparent electron excitation cross sections for 63 levels of the helium atom. The increase in apparent cross section of the singlet  $P$  levels with pressure can be explained by the imprisonment of resonance radiation; yet, nonresonance levels such as the singlet and triplet  $D$  show an equally strong pressure effect. Since the early work of Lees and Skinner<sup>1</sup> and Maurer and Wolf<sup>2</sup> it has been apparent that some mechanism such as collisional excitation transfer and/or radiative transition was transferring excitation from the  $^1P$  to the  $D$  levels. In later work, Gabriel and Heddle<sup>3</sup> and St. John *et al.*<sup>4,5</sup> introduced various models to explain the observed pressure dependence of the low  $nD$  levels. Other workers, Kay and Hughes<sup>6</sup> and Anderson *et al.*,<sup>7</sup> have used such models along with time-resolved spectroscopy to further study excitation transfer. Abrams and Wolga<sup>8</sup> have also investigated excitation transfer in helium by perturbing selected excited states through stimulated emission and observing the effect on other excited-state populations.

Excitation transfer from state  $j$  to state  $k$  may occur upon collision of an excited atom with a ground-state atom provided that the energy of relative motion is at least as great as the energy difference  $\Delta E$  between the initial and final excited states. Such a process will thus be rare for states separated in energy much greater than  $kT$ . For

this reason excitation transfer obeys the rule  $\Delta n = 0$  in helium unless  $n$  is greater than about 12. Theoretical considerations show that the cross section for excitation transfer also depends upon  $\Delta E$  and upon  $\Delta L$ , the change in orbital angular momentum occurring during the collision. Bates<sup>9</sup> and Stueckelberg<sup>10</sup> have derived expressions which indicate that the excitation-transfer cross sections increase as  $\Delta E$  decreases. Stueckelberg's formula however breaks down for small  $\Delta E$  in some cases.<sup>11</sup> Lin and Fowler<sup>12</sup> have shown that the transfer for  $\Delta L = \pm 2$  is stronger than for  $\Delta L = \pm 1, \pm 3$  and have used Stueckelberg's formula to estimate a cross section of about  $1 \times 10^{-14} \text{ cm}^2$  for  $4^1P \rightarrow 4^1F$  transfer. Chan<sup>13</sup> has applied Stueckelberg's formula to the  $4^3P \rightarrow 4^3D$  transfer and estimated a cross section of about  $2 \times 10^{-15} \text{ cm}^2$ . The Wigner spin rule<sup>14</sup>  $\Delta S = 0$  has been shown to hold for states with good Russell-Saunders coupling<sup>8</sup> and thus excitation transfer involving a change of multiplicity between such states may be neglected.

The apparent cross sections for electron excitation of the  $^1S$  and  $^3S$  levels generally show the smallest dependence on pressure followed by the  $^3P$  levels. The  $^1P$ ,  $^3D$ ,  $^1D$ , and  $F$  levels however show considerable pressure dependence and are the primary object of this study. Previous experimental work has been restricted to the behavior of relatively few low- $n$  levels such as the  $n^1P$  and  $nD$  levels with  $n=3, 4$ , or  $5$ . The experimental data to be described here are obtained from observations on the radiation from the following 63 levels:

$$\begin{array}{ll} n^1S, & n=3-10, & n^3S, & n=3-10, \\ n^1P, & n=2-10, & n^3P, & n=2-10, \end{array}$$

$$n^1D, \quad n=3-13, \quad n^3D, \quad n=3-13, \\ nF, \quad n=4-10.$$

## II. EXPERIMENTAL TECHNIQUE

The basic experimental apparatus<sup>15</sup> and associated electronics<sup>16</sup> have been described in previous papers. The fundamental experimental quantity of interest obtained from observation of the radiation from level  $j$  to level  $k$  is the *optical* cross section for electron excitation  $Q(jk)$  or simply optical cross section, with electron excitation understood. The *level* cross section  $Q(j)$  is that due to electron excitation only and may be obtained from  $Q(jk)$  by taking into account such processes as (a) cascade, i. e., radiative transitions ending on level  $j$ , (b) collisional transfer into and out of the level, (c) the availability of several channels for radiative decay, (d) polarization of the emitted radiation, and (e) imprisonment of resonance radiation. The *apparent* cross section  $Q'(j)$  of level  $j$  is the sum of the optical cross sections of transitions having a common upper level, i. e., taking into account only correction (c). The apparent cross section may be obtained from the optical cross section by using the branching factor  $B(jk)$  through the relation

$$\frac{Q'(j)}{Q(jk)} = B(jk) \equiv \frac{A(j)}{A(jk)}, \quad (1)$$

where  $A(jk)$  is the transition probability for dipole radiation from level  $j$  to level  $k$  and  $A(j)$  is the total transition probability from level  $j$ .

The optical cross section of a particular radiative transition is proportional to the integrated photon flux or photon rate  $F(jk)$  emitted by the  $j-k$  transitions as the electron beam traverses a length  $L$  of the gas in the collision chamber. The relation is

$$F(jk) = Q(jk)(I/e)NL, \quad (2)$$

where  $I$  is the electron beam current,  $e$  is the electron charge, and  $N$  is the gas ground-state number density. In practice, excited-state radiation originating in a thin slab of thickness  $L$  and area  $S$  is detected. For electron guns having cylindrical symmetry, the density of atoms in state  $j$  at radial distance  $R$  from the beam center may be denoted by  $N(j, R)$ . Then the total photon rate for the  $j-k$  transition emitted in length  $L$  of the beam will also be given by

$$F(jk) = 2\pi A(jk)L \int_0^\infty N(j, R)R dR. \quad (3)$$

Considering also that the current density  $J(R)$  in the beam may depend on  $R$  Eq. (2) may be written in general form as

$$Q(jk)(N/e) \int_0^\infty J(R)R dR = A(jk) \int_0^\infty N(j, R)R dR. \quad (4)$$

From Eq. (4) we see that the optical cross sections will be independent of the excited-state density distribution as long as  $S$  is made large enough so that  $N(j, R)$  is zero outside of  $S$ . Care was exercised in this work to make certain that the area  $S$  viewed by the optical system extended to the walls of the collision chamber. This becomes especially important at the higher gas pressures where the excitation associated with the imprisonment halo may extend a considerable distance from the beam itself. Care was also exercised in measuring the entire beam current. For convenience in writing population equations for excited states, it is customary to take the integral on the right-hand side of Eq. (4) as equal to  $N(j)S$ , where  $N(j)$  is an average excited-state density. Equation (4) may then be written

$$Q(jk)(IN/eS) = N(j)A(jk). \quad (5)$$

The apparent cross section for state  $j$  thus becomes

$$Q'(j) = N(j)B(jk)A(jk)(eS/IN). \quad (6)$$

The photon rate  $F(jk)$  is determined absolutely through a calibration procedure<sup>16</sup> which involves the observation by the detection system of light from a tungsten-ribbon standard lamp which has a photon radiance  $R(\lambda, T, \Delta\lambda)$ . The quantity  $R(\lambda, T, \Delta\lambda)$  is the rate of emission of photons by the standard lamp per unit source area in the wavelength range transmitted by the monochromator  $\lambda \pm \Delta\lambda$  at true temperature  $T$ . The determination of  $R(\lambda, T, \Delta\lambda)$  depends upon Plank's blackbody formula, the emissivity of tungsten, and the transmittance of the monochromator, this latter quantity being a triangular distribution with half-height width of  $\Delta\lambda$  when equal entrance and exit slits are used. Determinations must be made of the radiation source area  $A_s$  of the standard lamp, the solid angles of observation of the collision chamber and standard source  $\Omega_c$  and  $\Omega_s$ , the transmittances  $\gamma_c$  and  $\gamma_s$  of the detection system for the two beams, and the output signals  $I_c$  and  $I_s$  of the detector due to observation of the collision chamber and standard lamp, respectively. St. John<sup>17</sup> gives further details of the standardization procedure which show that the above quantities relate as

$$F(jk) = 4\pi A_s R(\lambda, T, \Delta\lambda) \frac{\Omega_s \gamma_s}{\Omega_c \gamma_c} \frac{I_c}{I_s}. \quad (7)$$

From Eqs. (2) and (7) the optical cross section may be expressed in terms of measurable quantities as

$$Q(jk) = KR(\lambda, T, \Delta\lambda) \frac{e}{IN} \frac{I_c}{I_s}, \quad (8)$$

where  $K$  is primarily a geometrical factor given by

$$K = 4\pi \frac{A_s \Omega_s \gamma_s}{L \Omega_c \gamma_c} \quad (9)$$

The transmittance ratio  $\gamma_s/\gamma_c$  is made equal to unity by adjusting the optical path of photons from the collision chamber to agree with that of photons from the standard lamp. Thus a plate of quartz equal in thickness to the quartz window in the standard lamp envelope was interposed between the collision chamber and monochromator during  $I_c$  determinations. The quantity  $L$  is determined by the entrance slit width while  $A_s$  was determined by an auxiliary slit. Measurements of these and of the magnifications of the lens system forming the images on the entrance slit were made for the determination of  $L$  and  $A_s$ .

The solid-angle ratio is determined by limiting apertures of diameter  $D_s$  and  $D_c$  for the standard source and collision chamber, respectively. For example, when the sources are at equal distances from the entrance slit,  $\Omega_s/\Omega_c = D_s^2/D_c^2$ . Considering the error involved in measuring the above quantities, the total error in  $K$  is  $\pm 5\%$ .

The emissivity data reported by De Vos<sup>18</sup> was used to make the nonblackbody corrections to the quantity  $R(\lambda, T, \Delta\lambda)$ . The true temperature  $T$  of the lamp as a function of current through the lamp was supplied by the lamp manufacturer.<sup>19</sup> The passband of the monochromator  $\Delta\lambda$  was determined from the monochromator relation

$$\Delta\lambda = s \cos\theta / f N_g, \quad (10)$$

where  $s$  is the entrance and exit slit dimension,  $f$  the focal length,  $N_g$  the grating ruling density, and  $\theta$  the angle between the grating normal and the exit slit. The quantity  $\Delta\lambda$  was checked by scanning across a discrete spectral line and measuring the base width  $2\Delta\lambda$  of the triangular transmission pattern produced. An estimate of the accuracy of  $R(\lambda, T, \Delta\lambda)$  was made by measuring the ratio of this quantity to the signal  $I_s$  which it produced as  $T$  was varied at constant wavelength. If  $R(\lambda, T, \Delta\lambda)$  indeed represented the true photon rate the ratio  $R(\lambda, T, \Delta\lambda)/I_s$  should remain constant. This procedure was carried out for different wavelengths over the spectral range investigated where a maximum ratio change of about  $\pm 4\%$  was found when the photon rates were changed by an order of magnitude. It was extremely important in the above determinations to ensure that monochromator light scatter was eliminated by proper broad-band spectral isolation filters, especially below 3500 Å.

The photon rates from the standard lamp and collision chamber were chopped at the same rate and the resulting detector signals were processed in a phase-sensitive lock-in amplifier. The output signals  $I_c$  and  $I_s$  of the lock-in amplifier were recorded on a strip chart recorder. When signal-to-noise

ratio was high, the error in these signals was primarily due to amplifier nonlinearity and was less than 0.5%.

The optical cross sections which are reported herein were determined at a relatively high pressure where  $N$  could be measured to within  $\pm 3\%$  using a rather large McLeod gauge with a 50-cm scale. Polarization corrections are negligible at high pressure because of collisional depolarization. The error associated with the measurement of  $I$  was no more than  $\pm 1\%$ . The possible total error in the absolute determinations of  $Q(jk)$  caused by the factors mentioned above may therefore be estimated to be  $\pm 14\%$  for the large majority of optical cross sections measured.

### III. EXPERIMENTAL RESULTS

Absolute values for the optical cross sections were obtained by the procedure outlined above at 63 mTorr pressure, 8 mA beam current, 100 eV electron energy, and a gas temperature of 300 °K. The results are given in Table I. The light detectors used in the various spectral ranges were EMI 6256B photomultiplier, 3000–6000 Å; EMI 9558B photomultiplier, 5000–8000 Å; RCA 7102 photomultiplier (77 °K), 7000–11 000 Å; Precision Industries PbS detector (77 °K), 10 000–21 000 Å; Kodak Ektron PbS detector, 18 000–21 000 Å. Operating temperature when different from ambient is noted. In the ultraviolet (uv) and visible regions a Jarrell-Ash  $\frac{1}{2}$ -m monochromator was used with a grating blazed at 5000 Å. In the infrared region, a Jarrell-Ash  $\frac{1}{4}$ -m monochromator was used with gratings of 12 000 and 21 000 Å blaze.

The measurements of  $Q(jk)$  in the visible and uv regions were reasonably straightforward. However, the transitions from the  $F$  levels in the infrared are somewhat complicated by the presence of unresolvable components. It was not possible to resolve the  $F$  radiation into its  $n^1F - 3^1D$  and  $n^3F - 3^3D$  components which are separated by less than 10 Å. Thus combined cross sections of the form  $Q(nF, 3D)$  are reported for these transitions. The  $nF$  cross sections,  $n \geq 5$ , must be corrected for the presence of the unresolved nearby transitions  $n^1P - 3^1D$ . The contribution from these lines to the total line intensity measured is only 5% or less and may be obtained from the observed  $Q(n^1P, 2^1S)$  by multiplying it by the ratio  $A(n^1P, 3^1D)/A(n^1P, 2^1S)$ . The line at 9528 Å however is mostly  $7^3D - 3^3P$  radiation and only 30% is from the  $8F - 3D$  transition. This large correction causes a greater uncertainty in the value of  $Q(8F, 3D)$ . The transitions from the higher  $F$  states are shown in the spectral scan of Fig. 1 obtained by use of the RCA 7102 photomultiplier tube.

The spectral range of the RCA 7102 tube overlapped that of the PbS detector used to measure

TABLE I. Absolute optical and apparent cross sections of helium at 63 mTorr pressure, 100 eV electron energy, and 8 mA beam current.

$\lambda$ (Å)	$k j$	$Q(jk)$ ( $10^{-20} \text{cm}^2$ )	$A(jk)$ ( $10^6 \text{sec}^{-1}$ )	$B(jk)$	$Q'(j)$ ( $10^{-20} \text{cm}^2$ )
7 065	$2^3P-3^3S$	24.2±3.4	27.8	1.00	24.2±3.4
4 713	$4^3S$	3.44±0.48	10.6	1.61	5.5±0.8
4 121	$5^3S$	1.21±0.18	4.30	2.10	2.5±0.4
3 867	$6^3S$	0.61±0.09	2.36	2.36	1.4±0.2
3 733	$7^3S$	0.28±0.04	1.55	2.46	0.70±0.14
3 652	$8^3S$	0.096±0.014	1.08	2.55	0.24±0.05
3 599	$9^3S$	0.029±0.004	0.75	2.63	0.075±0.018
3 563	$10^3S$	0.011±0.001	0.54	2.70	0.031±0.008
7 281	$2^1P-3^1S$	52.0±7.3	18.1	1.00	52.0±7.3
5 048	$4^1S$	10.2±1.4	6.55	1.69	17.2±2.6
4 438	$5^1S$	3.6±0.5	3.12	2.12	7.6±1.2
4 169	$6^1S$	1.2±0.2	1.76	2.36	2.8±0.5
4 024	$7^1S$	0.45±0.06	1.09	2.46	1.1±0.2
3 936	$8^1S$	0.18±0.03	0.72	2.64	0.48±0.12
3 878	$9^1S$	0.075±0.011	0.52	2.70	0.20±0.05
3 838	$10^1S$	0.027±0.004	0.38	2.75	0.074±0.017
0 830	$2^3S-2^3P$	170.0±24	10.22	1.00	170±24
3 889	$3^3P$	32.8±4.6	9.478	1.11	36.4±5.8
3 188	$4^3P$	13.4±2.0	5.93	1.27	17.0±3.0
2 945	$5^3P$	5.55±0.78	3.38	1.39	7.7±1.5
2 829	$6^3P$	2.58±0.36	2.04	1.47	3.8±0.7
2 764	$7^3P$	1.35±0.19	1.32	1.54	2.1±0.4
2 723	$8^3P$	0.68±0.09	0.89	1.61	1.1±0.2
2 696	$9^3P$	0.34±0.07	0.64	1.65	0.56±0.2
2 677	$10^3P$	0.17±0.05	0.48	1.68	0.29±0.1
20 581	$2^1S-2^1P$	679±95	1.976	901	(6.11±0.90)×10 <sup>5</sup>
5 016	$3^1P$	327±46	13.38	43.2	(1.41±0.21)×10 <sup>4</sup>
3 965	$4^1P$	65.2±9.1	7.17	35.6	(2.32±0.35)×10 <sup>3</sup>
3 613	$5^1P$	13.1±1.8	3.93	33.7	442±75
3 448	$6^1P$	3.3±0.5	2.39	32.5	107±18
3 355	$7^1P$	1.3±0.2	1.51	32.4	42±8
3 297	$8^1P$	0.66±0.10	1.02	32.1	21±4
3 258	$9^1P$	0.36±0.05	0.74	31.9	11±2
3 231	$10^1P$	0.20±0.03	0.55	31.8	6.3±1.2
5 876	$2^3P-3^3D$	54.5±7.5	70.6	1.00	54.5±7.5
4 471	$4^3D$	19.6±2.7	25.1	1.27	24.9±4.5
4 026	$5^3D$	13.7±1.9	11.7	1.39	19.1±4.0
3 820	$6^3D$	8.70±1.2	6.72	1.50	13.0±3.1
3 705	$7^3D$	4.87±0.70	4.14	1.56	7.6±1.7
3 634	$8^3D$	2.55±0.36	2.73	1.62	4.1±1.0
3 587	$9^3D$	1.45±0.21	1.80	1.67	2.4±0.6
3 554	$10^3D$	0.76±0.11	1.31	1.70	1.3±0.3
3 532	$11^3D$	0.38±0.05	0.98	1.72	0.65±0.15
3 514	$12^3D$	0.20±0.03	0.75	1.73	0.35±0.08
3 500	$13^3D$	0.11±0.01	0.59	1.73	0.19±0.04
6 678	$2^1P-3^1D$	74.5±10	63.8	1.00	74.5±10
4 922	$4^1D$	31.7±4.5	20.2	1.34	42.5±7.5
4 388	$5^1D$	11.9±1.7	9.07	1.53	18.2±3.5
4 144	$6^1D$	4.30±0.60	4.88	1.63	7.0±1.4
4 009	$7^1D$	1.80±0.25	2.96	1.78	3.2±0.7
3 927	$8^1D$	0.82±0.12	1.94	1.82	1.5±0.3
3 872	$9^1D$	0.45±0.06	1.33	1.85	0.83±0.20
3 834	$10^1D$	0.24±0.03	0.96	1.86	0.44±0.11
3 805	$11^1D$	0.14±0.02	0.70	1.87	0.26±0.06
3 784	$12^1D$	0.085±0.01	0.52	1.88	0.16±0.04
3 768	$13^1D$	0.053±0.01	0.40	1.88	0.10±0.03

TABLE I. (Continued)

$\lambda$ (Å)	$k j$	$Q(jk)$ ( $10^{-20}$ cm $^2$ )	$A(jk)$ ( $10^6$ sec $^{-1}$ )	$B(jk)$	$Q'(j)$ ( $10^{-20}$ cm $^2$ )
18 690	3D-4F	64.0 ± 9.0	13.7	1.00	64.0 ± 9.0
12 787	5F	20.3 ± 2.8	4.51	1.59	32.3 ± 5.5
10 914	6F	4.74 ± 0.67	2.14	1.94	9.2 ± 1.5
10 029	7F	1.90 ± 0.27	1.22	2.22	4.2 ± 0.7
9 528	8F	0.50 ± 0.20	0.75	2.40	1.2 ± 0.5
9 212	9F	0.37 ± 0.05	0.50	2.49	0.92 ± 0.20
8 997	10F	0.21 ± 0.03	0.34	2.58	0.54 ± 0.12

$Q(2^3P, 2^3S)$  and also overlapped the spectral range of the EMI 9558 photomultiplier used to measure  $Q(3^1S, 2^1P)$ . The values of these two optical cross sections were redetermined using the RCA 7102 tube and the agreement was found to be within 10%, a value well within our estimated error limits of  $\pm 14\%$ . Another check on the consistency of our optical system calibration over such a large spectral range involved an independent determination of  $Q(4F, 3D)$ . The  $4^1D \rightarrow 3^1P$  radiation at 19 089 Å was easily detected and lies close enough to the  $4F \rightarrow 3D$  radiation at 18 690 Å for the standardization parameters to be considered equal. Hence  $Q(4F, 3D)$  may be determined from Eq. (8) as

$$Q(4F, 3D) = Q(4^1D, 3^1P) I_c(18\,690)/I_c(19\,089).$$

The optical cross section  $Q(4^1D, 3^1P)$  may be determined from the independently measured visible transition  $Q(4^1D, 2^1P)$  through multiplication by the ratio  $A(4^1D, 3^1P)/A(4^1D, 2^1P)$  according to Eq. (5). These transition probabilities are accurate to within about 5% and the published values from three sources<sup>6,20,21</sup> lie within this range. In the above manner  $Q(4F, 3D)$  was found to be  $63 \times 10^{-20}$  cm $^2$  which compares well with the value from Table I.

The accuracy of the apparent cross sections given in Table I is of course less than the accuracy of the optical cross sections because of the additional error in the branching factors caused by an inaccurate knowledge of the transition probabilities involved. For the S, P, and D levels the most extensive published values of transition probabilities are those given by Wiese *et al.*,<sup>20</sup> Niles,<sup>21</sup> and Gabriel and Heddle.<sup>3</sup> Some of the transition probabilities listed by Wiese *et al.* have accuracies as good as 1%; however, the majority are in the 5 or 10% accuracy range. The values tabulated by Niles were obtained by examining literature values, by graphical smoothing and extrapolation methods, and by comparing hydrogen and helium transition probabilities. The discrepancy between 120 values of  $A(jk)$  given by both Wiese *et al.* and Niles was found to have an average value of 5%. In the present work values of  $A(jk)$  given by Wiese *et al.* were

used when the stated accuracy was  $\leq 5\%$ . The remaining values of  $A(jk)$  for  $k$  up to 4S, 4P, and 4D and initial states up to  $n=15$  were taken from the work of Niles. Hydrogenic transition probabilities were computed for the F to D transitions. These values, given in Table II, were calculated using the hypergeometric-series solution of the radial integral as outlined by Condon and Shortley.<sup>22</sup> Values given were calculated up to  $n=10$  and extrapolated to  $n=12$ . Care must be exercised in extrapolation since the usual  $n^{-3}$  behavior is not sensibly approached until  $n$  becomes very large; e.g., at  $n=10$  the values  $A(nF, 3D)$  vary as  $n^{-3.6}$  and at  $n=25$  as  $n^{-3.1}$ . The values show close agreement with the few available corresponding Coulomb-approximation values<sup>20</sup> and probably represent the helium transition probabilities to within 5%. Errors due to the branching ratios given in Table I can be estimated to range from 0 [ $B(jk)=1.00$ ] to  $\sim 10\%$  and the error limits on the apparent cross sections therefore vary from 14 to  $\sim 25\%$ .

Branching ratios used for terminal levels with

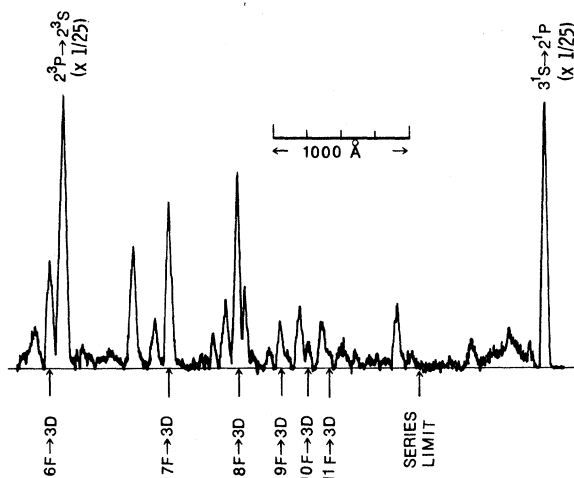


FIG. 1. Spectral scan showing lines from the higher  $nF \rightarrow 3D$  transitions at 63 mTorr pressure, 100 eV electron energy, and 8 mA beam current. The two strong lines as shown are attenuated by a factor of 25.

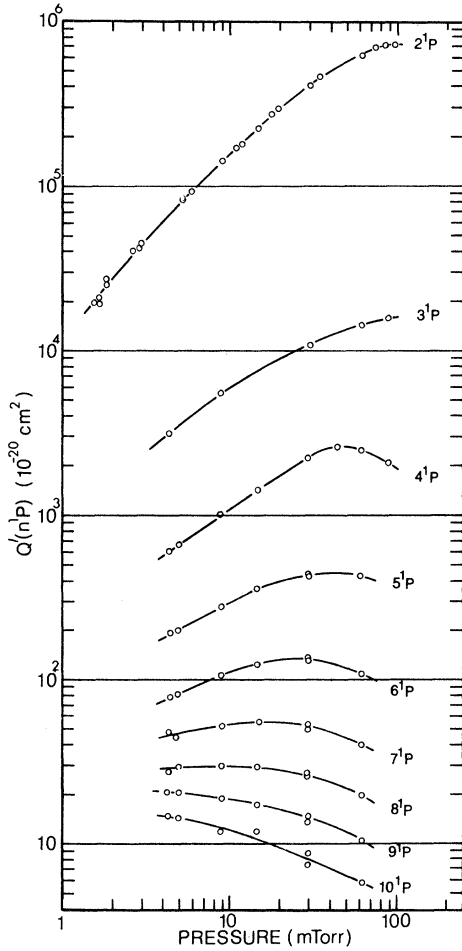


FIG. 2. Pressure dependence of the apparent cross sections of the  $n^1P$  levels.

$n > 4$  for the  $S$ ,  $P$  and  $D$  levels were obtained from the Coulomb-approximation values given by Gabriel and Heddle<sup>3</sup> which are tabulated up to  $n = 8$ . Extrapolations of these values were used when transition probabilities involving levels with  $n = 9$  or greater were needed. In all cases the branching ratios tended to approach limiting values as the initial-level principle quantum number increased.

The pressure variation of the apparent cross sections of the various levels for 100-eV electrons was determined by the variation of the detector signal  $I_c$  with pressure at constant electron beam current  $I$ . These data are presented in Figs. 2–5. For the  $3^1P$  level, we were able to determine  $Q'(3^1P)$  over the pressure range 100–0.01 mTorr. This curve is shown in Fig. 6. The  $3^1P$  data have been corrected for polarization of the 5016-Å radiation. Instrumental polarization at this wavelength is negligible. The solid line through the data is computed from imprisonment theory which will be presented later. An accurate means was used for de-

termining the ground-state density in the collision chamber at pressures below about 5 mTorr for the  $3^1P$  level. The  $5^1S \rightarrow 2^1P$  radiation per unit beam current at 32 eV was found to be linear with pressure over the range 5–100 mTorr. This linearity may be expected to hold at lower pressures since the  $5^1S$  level at 32 eV is not appreciably affected by polarization, cascade, or excitation transfer. The ratio  $I_c/I$  was thus used to determine the pressure in the collision chamber down to about 0.01 mTorr. This procedure eliminates two major sources of error connected with low-pressure measurements. One source deals with mercury-streaming corrections to the McLeod gauge. The other is due to the departure of the collision-chamber temperature from ambient observed at low pressure. This latter effect is caused by the thermal isolation of the collision chamber from the vacuum-chamber walls as helium gas is removed and can lead to error in calculating  $N$  from the gas law.

#### IV. DATA ANALYSIS AND INTERPRETATION

##### A. General Populating Processes

The processes which may affect the population of a level  $j$  written in terms of gain and loss rates per unit volume are as follows: radiative loss,  $N(j)A(j)$ ; net transfer gain,  $\bar{c}N\sum_k[N(k)Q_t(k \rightarrow j) - N(j)Q_t(j \rightarrow k)]$ ; electron excitation gain,  $Q(j)(IN/eS)$ ; radiative gain (cascade),  $\sum_i N(i)A(jk)$ ; imprisonment gain,  $(1-g)N(j)A(j, 1^1S)$ . In these expressions,  $\bar{c}$  is the relative velocity of the interacting atoms and  $g$  is the fraction of resonance photons which escape to the collision-chamber walls without being absorbed. The velocity-averaged transfer cross section between two levels is  $Q_t(j \rightarrow k)$  and is

TABLE II. Hydrogenic-transition probabilities (first row) in units of  $10^6 \text{ sec}^{-1}$  and inverse-branching ratios (second row) for  $F \rightarrow D$  transitions.

	4F	5F	6F	7F	8F	9F	10F	11F <sup>a</sup>	12F <sup>a</sup>
3D	13.70	4.51	2.14	1.22	0.750	0.501	0.344	0.250	0.185
	1.00	0.630	0.515	0.452	0.416	0.403	0.386	0.380	0.378
4D		2.56	1.29	0.729	0.458	0.308	0.218	0.150	0.110
		0.370	0.310	0.271	0.252	0.247	0.232	0.227	0.225
5D			0.720	0.420	0.272	0.186	0.129	0.094	0.070
			0.175	0.159	0.150	0.144	0.142	0.141	0.141
6D				0.320	0.192	0.116	0.081	0.053	0.042
				0.118	0.106	0.095	0.089	0.082	0.082
7D					0.142	0.082	0.060	0.042	0.028
					0.076	0.065	0.065	0.064	0.063
8D						0.059	0.043	0.030	0.020
						0.047	0.046	0.045	0.043
9D							0.033	0.022	0.015
							0.037	0.034	0.031
10D								0.017	0.011
								0.026	0.023
11D									0.008
									0.016

<sup>a</sup>Extrapolated values.

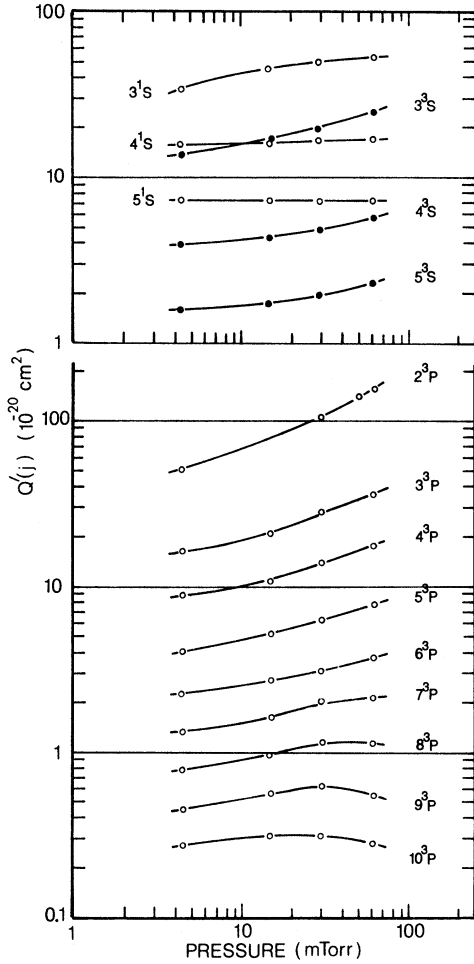


FIG. 3. Pressure dependence of the apparent cross sections of the  $n^1S$ ,  $n^3S$ , and  $n^3P$  levels.

related to the transfer cross section for the reverse process through the statistical weights  $w$ , so that

$$Q_t(j \rightarrow k) = b(kj)Q_t(k \rightarrow j), \quad (11)$$

where  $b(kj)$  is defined as

$$b(kj) = w(k)/w(j). \quad (12)$$

Equation (11) of course assumes that the transfer reaction occurs with equal probability between any pair of the  $2J+1$  degenerate states in the levels involved. A steady-state population equation for a given state is obtained by equating the loss term to the sum of the gain terms. In some situations, some gain terms may be negligible.

The gain and loss terms may be expressed in terms of the more fundamental measured quantities, the apparent cross sections, through multiplication by  $eS/IN$ , use of

$$N(j) = \frac{Q'(j)}{A(j)} \frac{IN}{eS}$$

from Eqs. (1) and (5), and by use of Eq. (11). The resulting terms may be then defined as follows:

radiative loss,  $Q'(j)$ ;

net-transfer gain,

$$Q^*(j) = \sum_k Q^*(k \rightarrow j) \\ = \bar{c}N \sum_k Q_t(k \rightarrow j) [Q'(k)/A(k) - b(kj)Q'(j)/A(j)]; \quad (13)$$

electron excitation gain,  $Q(j)$ ;

radiative gain,

$$Q_c(j) = \sum_i Q'(i)B^{-1}(ij); \quad (14)$$

imprisonment gain,

$$Q_i(j) = (1-g)Q'(j)B^{-1}(j, 1^1S). \quad (15)$$

All gain terms except those arising from electron excitation may be pressure dependent and only in the limit of "zero" pressure do we have  $Q'(j) = Q(j) + Q_c(j)$ .

The analysis of the experimental data includes a qualitative explanation of the variation of apparent cross section with pressure and a quantitative determination of the various gain and loss terms at 63 mTorr, 100 eV, and 8 mA. In the determination of such terms as  $Q^*(j)$  the error involved is estimated from relative errors in the apparent cross sections used rather than the absolute error discussed in the last section. Some of the mitigating factors which serve to reduce the relative errors include the fact that  $N$  and  $I$  were held constant during data acquisition. In addition, the factor  $K$  remained constant for each monochromator used. The relative error between  $Q'(j)$  values for  $n > 4$  in a particular series is further reduced because of the slight variation in  $R(\lambda, T, \Delta\lambda)$  over the wavelength range involved. Such considerations have been used to assign the best estimate of the most probable error in the determination of  $Q^*(j)$ .

#### B. $1^3P$ Levels

The effect of pressure on the apparent cross sections of the  $1^3P$  family is seen from Fig. 2. The curves tend to rise with pressure because of the additional populating effect of resonance-radiation imprisonment as given by  $Q_i(j)$ . Beginning with the  $4^3P$  level, a decrease with increasing pressure is observed indicating that collisional excitation transfer becomes progressively more important as a depopulating mechanism with increasing  $N$ . The  $2^3P$  and  $3^3P$  curves show little or no depopulating effect. This is to be expected for the  $2^3P$  level since this level is separated from other levels by an energy difference much greater than  $kT$ . However, for the  $3^3P$  and higher levels, an excitation transfer reaction becomes energetically possible. The magnitude of the excitation transfer may be evaluated

by an analysis of the steady-state equation for the level of interest.

The steady-state equation obtained by equating gain and loss rates for a  $n^1P$  level may be written as

$$Q'(n^1P) = Q_{ec}(n^1P) + Q_i(n^1P) + Q^*(n^1P), \quad (16)$$

where

$$Q_{ec}(n^1P) = Q(n^1P) + Q_c(n^1P) \quad (17)$$

and

$$Q^*(n^1P) = \sum_k Q^*(k \rightarrow n^1P). \quad (18)$$

The transfer gain term is thus given by

$$Q^*(n^1P) = Q'(n^1P) - (1-g)B^{-1}(n^1P, 1^1S)Q'(n^1P) - Q_{ec}(n^1P). \quad (19)$$

In order to evaluate the transfer gain term it is necessary to obtain values for  $g$  and  $Q_{ec}(n^1P)$ . The value of  $Q_{ec}(3^1P)$  is determined directly from the low-pressure limit of  $Q'(3^1P)$  shown in Fig. 6. Phelps<sup>23</sup> has calculated expressions for limiting values of  $g$  for a collision chamber of cylindrical symmetry with radius  $R$  and has shown that the exact value of  $g$  differs from the mean of these limits by less than 5%. We will adopt this mean value of  $g$  which is given in Ref. 3 as a function of the product  $k_0R$ , where  $k_0$  is the absorption coefficient at the line center for a line subject to Doppler broadening only. In practice the collision chamber is usually nearly enclosed at both ends, contains viewing windows, etc., so that one no longer has ideal cylindrical symmetry. Under such conditions it is necessary to obtain an effective radius  $\rho$  which

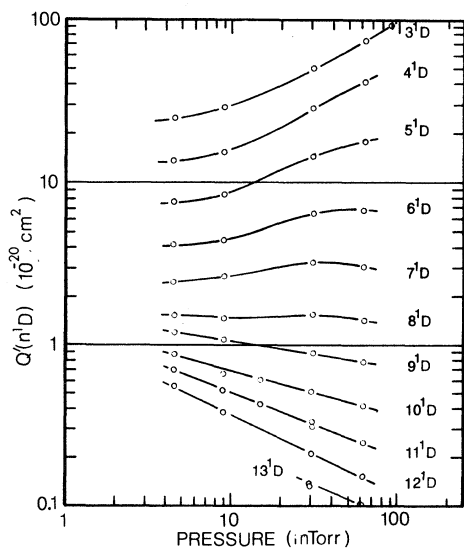


FIG. 4. Pressure dependence of the apparent cross sections of the  $n^1D$  levels.

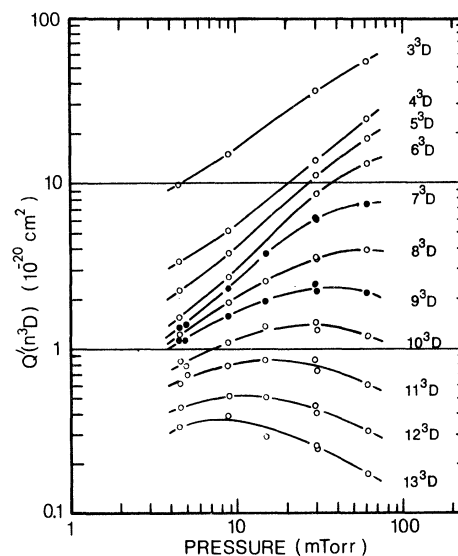


FIG. 5. Pressure dependence of the apparent cross sections of the  $n^3D$  levels.

is characteristic of a particular collision-chamber geometry and which may be used in place of  $R$ . We have used the data for the  $3^1P$  level shown in Fig. 6 to determine  $\rho$  for our collision chamber. By examining Eq. (19) at 0.01 ( $g \sim 1$ ) and 100 mTorr ( $g \sim 0$ ),  $Q^*(3^1P)$  was found to be negligible. At the intermediate pressures the shape of the pressure curve is strongly dependent upon the imprisonment radius  $\rho$ . It was determined that a value of  $\rho = 0.75$  cm yields a pressure curve from Eq. (19) which agrees with the best-fit curve of the experimental data to within 5% over the entire pressure range. Since the imprisonment radius depends only upon the fixed geometry of the collision chamber, it may be assumed to remain constant for other levels of the resonance series. The above process of obtaining  $\rho$  by fitting to the observed  $Q'(3^1P)$  over a wide range of pressures is felt to be considerably more accurate than either the use of a similar method by Phelps<sup>23</sup> over a restricted pressure range or another method employed earlier by the present authors<sup>15</sup> for the  $2^1P$  level and by Gabriel and Heddle<sup>3</sup> for the  $3^1P$  level.

It was not possible to reach low-pressure limits for other  $1^1P$  levels due to weak signals. However, at a pressure of 4.5 mTorr  $Q_{ec}(n^1P)$  may be evaluated from Eq. (19) for the lower  $n^1P$  levels which are not significantly affected by collisional depopulation at this pressure, i.e., for  $Q^*(n^1P)$  negligible. In order to estimate the maximum magnitude of  $Q^*(n^1P)$  at 4.5 mTorr, we note that the maximum depopulating effect would occur by neglecting the collisional gain from other levels, in which case Eq. (13) reduces with the aid of Eq. (11) to

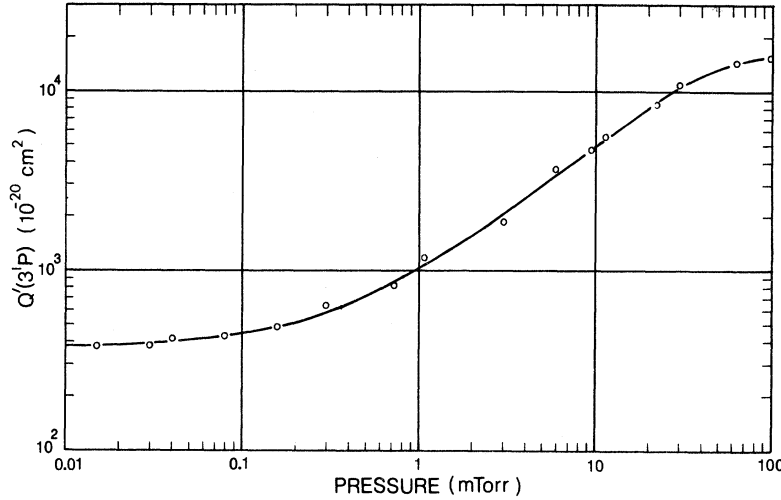


FIG. 6. Pressure dependence of the apparent cross section of the  $3^1P$  level. The solid curve is calculated from imprisonment theory. The data are measured cross section values.

$$Q^*(n^1P) = -\bar{c}N \frac{Q'(n^1P)}{A(n^1P)} \sum_k Q_t(n^1P-k). \quad (20)$$

An analysis of the  $D$  and  $F$  states presented in the following sections shows that we may expect transfer cross sections for the lower  $n^1P$  levels ( $n > 3$ ) to lie in the range  $10^{-14}$ – $10^{-13}$   $\text{cm}^2$ . Even for values as large as  $10^{-13}$   $\text{cm}^2$ , Eq. (20) indicates that  $Q^*(n^1P)$  is less than 3% of  $Q'(n^1P)$  for  $n=4, 5$ , and 6 and may become appreciable only for  $n \geq 7$ . Values of  $Q_{ec}(n^1P)$  for  $n=7-10$  were therefore obtained by extrapolation of the values for  $n=2-6$ , these latter values following closely a  $n^{-3.1}$  behavior.

In order to further verify that the above values of  $Q_{ec}(n^1P)$  exhibit the proper behavior with  $n$ , we made a comparison with excitation cross sections calculated from the Born approximation, a rather good approximation for the optically allowed transitions at energies  $\geq 100$  eV. Unfortunately, Born-approximation values are not available from the literature for the  $n^1P$  levels of large  $n$ . However, Kim and Inokuti<sup>24,25</sup> have shown that the Bethe procedure gives the Born cross section  $Q_B(j)$  to better than 1% for the 2, 3, and 4  $^1P$  levels at 100 eV when evaluated in the form

$$Q_B(j) = \frac{4\pi a_0^2}{T/R_\infty} \frac{f(n^1P)}{E(n^1P)/R_\infty} \left[ \ln \frac{4T}{R_\infty} + \ln c(n^1P) + \frac{\gamma(n^1P)}{T/R_\infty} \right], \quad (21)$$

where  $T$  is the electron energy,  $E(n^1P)$  is the excitation energy,  $f(n^1P)$  is the optical oscillator strength,  $R_\infty$  is the Rydberg constant,  $a_0$  is the Bohr radius and the parameters  $c(n^1P)$ ,  $\gamma(n^1P)$  depend upon the general oscillator strength. Kim and Inokuti have evaluated these parameters using highly accurate wave functions for the 2, 3, and 4  $^1P$  levels. Their values indicate that at 100 eV the sum of the last two terms in the brackets of Eq. (21) are  $-1.863$ ,  $-1.830$ , and  $-1.816$  for the three levels,

respectively. Because of the slow variation with  $n$  of these values, it is reasonable to assume that they remain constant at  $-1.816$  for  $n \geq 5$ , in which case the Born approximation of Eq. (21) gives at  $T=100$  eV with  $E(n^1P)$  in electron volts

$$Q_B(n^1P) = 1.016 \frac{f(n^1P)}{E(n^1P)} \times 10^{-15} \text{ cm}^2. \quad (22)$$

Oscillator strengths from the compilation by Wiese *et al.*<sup>20</sup> have been used to obtain  $Q_B(n^1P)$  from Eqs. (21) and (22) up to  $n=10$  and these values are given in Table III.

Cascade corrections to  $Q_{ec}(n^1P)$  are necessary before a valid comparison with the theoretical values may be made. The corrections amounts to 8% for the 2  $^1P$  and 3  $^1P$  levels and decreases as  $n$  increases. The theoretical and experimental cross sections are compared in the second and third columns of Table III and the agreement is within 10%. Much of the good agreement may be ascribed to the fact that the transition probabilities  $A(n^1P, 1^1S)$  used in obtaining  $Q(n^1P)$  from the experimental data and the oscillator strengths of Eqs. (21) and (22) are

TABLE III. Evaluation of excitation transfer-gain terms for the  $n^1P$  levels at 100 eV in units of  $10^{-20} \text{ cm}^2$ .

$j$	$Q_B(j)$	$Q(j)$	$Q_{ec}(j)$	$Q'(j) - Q_t(j)$	$Q^*(j)$
2 $^1P$	1280	1190	1290	...	...
3 $^1P$	319	350	374	384	$10 \pm 20$
4 $^1P$	129	145	158	103	$-55 \pm 16$
5 $^1P$	64.6	72	77	30	$-47 \pm 7$
6 $^1P$	35.6	41	43	10	$-33 \pm 4$
7 $^1P$	24.8	26	27 <sup>a</sup>	6	$-21 \pm 3$
8 $^1P$	16.6	17	18 <sup>a</sup>	4	$-14 \pm 2$
9 $^1P$	11.4	12	12 <sup>a</sup>	3	$-9 \pm 2$
10 $^1P$	8.7	9	9 <sup>a</sup>	2	$-7 \pm 2$
> 10 $^1P^a$	38	37	37	7	$-30 \pm 10$

<sup>a</sup>Extrapolated values.

TABLE IV. Evaluation of excitation transfer-gain terms for the  $^1S$ ,  $^3S$ , and  $^3P$  levels at 63 mTorr and 100 eV in units of  $10^{-20}$  cm $^2$ .

$j$	$Q_c(j)$		$Q(j)$	$Q_{ec}(j)$	$Q'(j)$	$Q^*(j)$	
	$S$	$D$					$P$
$3^3S$			8.8	11.2	20	24.2	$4.2 \pm 3$
$4^3S$			1.6	3.5	5.1	5.5	$0.4 \pm 0.7$
$5^3S$			0.4	1.6	2.0	2.5	$0.5 \pm 0.5$
$3^1S$			22	28	50	52	$2 \pm 4$
$4^1S$			2.1	15	17.1	17.2	$0.1 \pm 1.5$
$5^1S$			0.3	7.3	7.6	7.6	$0 \pm 0.3$
$2^3P$	30	106		25	161	170	$9 \pm 15$
$3^3P$	3.6	17.6		14	35	36.4	$1.4 \pm 3.5$
$4^3P$	1.0	4.8		7.4	13.2	17.0	$3.8 \pm 2.0$
$5^3P$	0.36	1.3		3.3	5.0	7.7	$2.7 \pm 1.0$
$6^3P$	0.16	0.45		1.9	2.5	3.8	$1.3 \pm 0.5$
$7^3P$	0.07	0.17		1.0	1.3	2.1	$0.8 \pm 0.4$
$8^3P$	0.03	0.07		0.7	0.8	1.1	$0.3 \pm 0.4$

based on essentially the same set of wave functions.<sup>20</sup> Moiseiwitsch and Smith<sup>26</sup> have tabulated experimental values resulting from five previous investigations for the  $3^1P$  and  $4^1P$  cross sections. Although these values show considerable spread because of systematic or other errors, the average values are 393 and  $163 \times 10^{-20}$  cm $^2$ , respectively, for  $Q_{ec}(3^1P)$  and  $Q_{ec}(4^1P)$ , which agree rather well with the present work.

Having obtained reliable values for  $Q_{ec}(n^1P)$ , the transfer-gain term is obtained from Eq. (19) evaluated at 63 mTorr. The quantities used in the evaluation are listed in the last three columns of Table III. The  $2^1P$  level was not evaluated since, as discussed by Phelps,<sup>23</sup> the imprisonment theory breaks down for this level at high pressures. The small amount of transfer gain shown for the  $3^1P$  level is not significant in view of the error involved. The net transfer gain terms for the higher levels are negative indicating a net transfer loss.

#### C. $^1S$ , $^3S$ , and $^3P$ Levels

The pressure variation of the  $nS$  levels,  $n=3-5$ , and the  $n^3P$  levels,  $n=2-10$ , are shown in Fig. 3. The  $S$  levels for high  $n$  were difficult to measure reliably at 100 eV and low pressure because the optical cross sections are somewhat small and the lines lie rather close to the stronger corresponding  $nD$  lines. The pressure variation shown is due in large part to cascading from higher levels as may be seen by an analysis of the steady-state equation

$$Q'(j) = Q_{ec}(j) + Q^*(j). \quad (23)$$

The transfer-gain term may be obtained by subtracting electron excitation and cascade gain from  $Q'(j)$ . The results at 100 eV and 63 mTorr are summarized in Table IV. The  $S$ ,  $D$ , and  $P$  cross sections needed for the cascade calculation and the  $Q'(j)$  cross sections are taken from Table I. The electron excitation terms  $Q(j)$  were determined by cascade cor-

rection of  $Q'(j)$  at 4.5 mTorr under the assumption of negligible collisional transfer at this pressure. The increasing error did not warrant extension of this analysis to  $n^3P$  levels higher than  $n=8$ .

The results indicate that electron excitation and cascading are sufficient to account for practically all of  $Q'(j)$  and that excitation transfer must be small, especially for the  $S$  levels. Since  $\Delta E$  is larger than  $kT$  up to  $n=7$  for the  $^3S$ - $^3P$  separation and up to  $n=6$  for the  $^1S$ - $^1P$  separation, little or no transfer should occur from these levels. Also, transfer of excitation involving the  $2^3P$  level is known to be zero because of similar energy considerations. Hence, the results obtained for these levels tend to validate our error estimation method.

The variation of  $Q'(n^3P)$  with pressure as shown in Fig. 3 is in general not as pronounced as found for the  $^1P$  and  $D$  levels. Much of the pressure dependence is due to pressure-dependent cascading from the  $^3D$  levels. This is in keeping with the fact that a direct transfer interaction with the  $^3D$  or  $F$  levels is not as likely for the  $^3P$  levels as a  $^1D$  or  $F$  interaction is with the  $^1P$  levels because of the larger energy difference involved in the  $^3P$  transfer.

#### D. $D$ Levels

For the  $D$  levels, with singlet and triplet levels considered together as one level, the steady-state equation may be written as

$$Q'(nD) = Q_{ec}(nD) + Q^*(nD). \quad (24)$$

The evaluation of  $Q^*(nD)$  is given in Table V. The transfer-gain term for the  $3D$  level is found to be zero, although the exact agreement between  $Q_{ec}(3D)$  and  $Q'(3D)$  is somewhat fortuitous in view of the error involved. Such a result is consistent with the earlier observation that the  $3^1P$  level failed to show significant transfer loss. From the error limits an upper limit to the value of  $Q_t(3^1P-3^1D)$  can be calculated as  $1.2 \times 10^{-15}$  cm $^2$ .

For the  $4D$  and higher levels  $F$  cascade is not suf-

TABLE V. Evaluation of excitation transfer-gain terms for the  $nD$  levels at 100 eV and 63 mTorr in units of  $10^{-20}$  cm $^2$ .

$j$	$Q_c(j)$		$Q(j)$	$Q_{ec}(j)$	$Q'(j)$	$Q^*(j)$
	$P$	$F$				
$3D$	5	96	28	129	129	$0 \pm 10$
$4D$	2	22	15	39	67	$28 \pm 5$
$5D$	0.7	3	8.5	12	37	$25 \pm 4$
$6D$	0.3	0.8	4.7	5.8	20	$14 \pm 3$
$7D$	0.13	0.2	2.9	3.2	11	$7.8 \pm 2$
$8D$	0.07	0.04	1.7	1.8	5.5	$3.7 \pm 1$
$9D$	0	0	1.1	1.1	3.1	$2.0 \pm 0.5$
$10D$	0	0	0.8	0.8	1.6	$0.8 \pm 0.3$
$>10D^a$	0	0	2.7	2.7	3.2	$0.5 \pm 0.7$

<sup>a</sup>Extrapolated values.

ficient to account for all the observed pressure dependence of  $Q'(nD)$ . This may be investigated in in some detail on the  $n=4$  level by writing the steady-state equations as

$$\begin{aligned} Q^*(4^1P) &= Q^*(4F \rightarrow 4^1P) + Q^*(4D \rightarrow 4^1P) \\ &= Q'(4^1P) - Q_{ec}(4^1P) - Q_t(4^1P), \end{aligned} \quad (25)$$

$$\begin{aligned} Q^*(4D) &= Q^*(4F \rightarrow 4D) + Q^*(4^1P \rightarrow 4D) \\ &= Q'(4D) - Q_{ec}(4D), \end{aligned} \quad (26)$$

$$\begin{aligned} Q^*(4F) &= Q^*(4D \rightarrow 4F) + Q^*(4^1P \rightarrow 4F) \\ &= Q'(4F) - Q_{ec}(4F). \end{aligned} \quad (27)$$

The  $4^3P$  interaction as given by  $Q^*(4^3P)$  is small and this level is neglected as a first approximation. Since  $Q^*(j \rightarrow k) = -Q^*(k \rightarrow j)$ , the above system of equations essentially has three unknowns; however, the equations are not independent and hence do not yield solutions for the transfer terms. There is evidence to indicate that the  $P \rightarrow D$  transfer is negligible and that the  $F \rightarrow D$  mechanism is responsible for  $Q^*(4D)$ . The energy difference between the  $P$  and  $D$  levels is much larger than for the  $F$  and  $D$  levels and excitation transfer should favor the latter route. In addition, a transfer of excitation from the  $^1P$  to the  $^3D$  portion of the  $4D$  level violates the spin rule. Abrams and Wolga<sup>8</sup> have also shown that a significant transfer of excitation does take place between the  $4F$  and  $4D$  levels although they were unable to determine the magnitude of the cross section involved. The  $F \rightarrow D$  mechanism has the added advantage that it does not violate the Wigner-spin rule since the spin of the  $F$  level is not well defined.<sup>12</sup> Assuming then that the  $P \rightarrow D$  transfer is negligible, Eq. (26) gives with the aid of Eq. (13)

$$\begin{aligned} Q_t(4F \rightarrow 4D) &= \frac{Q^*(4D)}{\bar{c}N} \left[ \frac{Q'(4F)}{A(4F)} - \frac{Q'(4D)}{b(4D, 4F)A(4D)} \right]^{-1} \\ &= (4.7 \pm 1.5) \times 10^{-14} \text{ cm}^2. \end{aligned} \quad (28)$$

In Eq. (28) the statistical weight ratio is 20/28 and the  $4D$  total transition probability is an average of  $A(4^1D)$  and  $A(4^3D)$ . In a similar manner, Eq. (25) gives, with  $Q^*(4D \rightarrow 4^1P)$  negligible,  $Q_t(4^1P \rightarrow 4F) = (2.1 \pm 0.5) \times 10^{-14} \text{ cm}^2$ . Evaluation of Eq. (27) will be reserved for Sec. IV E.

A detailed evaluation of the transfer mechanisms affecting  $D$  levels higher than  $n=4$  is not possible because sufficient data are lacking concerning possible interaction with  $G$ ,  $H$ , etc., levels. Nevertheless, the pressure curves of the  $D$  levels shown in Figs. 4 and 5 show distinct and gradual changes with  $n$  which qualitatively indicate the transfer processes occurring. The factors which affect the apparent cross sections of the  $D$  levels may be seen by solving the steady-state equation for  $Q'(nD)$  giving

$$Q'(nD) = \frac{Q_{ec}(nD) + \bar{c}N \sum_k [Q'(k)/A(k)] Q_t(k \rightarrow nD)}{1 + [\bar{c}N/A(nD)] \sum_k b(k, nD) Q_t(k \rightarrow nD)}. \quad (29)$$

In the above equation,  $k$  represents those levels such as  $nF$ ,  $nG$ , etc., which may interact collisionally with the  $nD$  levels. As the principal quantum number increases, there are three main effects on  $Q'(nD)$ . As can be seen from Table V, the cascade term becomes less important as  $n$  increases. In addition, judging by the decline of  $Q'(nF)/A(nF)$  with  $n$ , it is likely that the populations of other  $k$  levels also decrease somewhat as  $n$  increases. Also, the transition probabilities  $A(nD)$  decrease with increasing  $n$ . The second effect causes a reduction in the terms multiplying  $N$  in the numerator and the third effect causes an increase in the terms multiplying  $N$  in the denominator as  $n$  increases. The net result will be an increase of  $Q'(nD)$  with pressure due to cascade and transfer gain for the levels of low  $n$  and a decrease of  $Q'(nD)$  with increasing pressure due to net transfer loss for levels of high  $n$ . Thus, a level such as the  $8^1D$  may seem under cursory examination to be nearly free from pressure-dependent transfer processes when in fact it is an active participant with populating processes equal to depopulating processes over a wide range of pressures.

The primary difference between the  $^1D$  and  $^3D$  levels becomes apparent at the lower pressures where  $Q'(n^1D)$  is dominated by a relatively large electron-excitation term whereas the corresponding term for the triplet levels is much smaller.

#### E. $F$ Levels

The apparent cross sections of the  $F$  levels at 100 eV and 63 mTorr decrease approximately as  $n^{-6}$ , i. e., at about the same rate as observed for the  $^1P$  and  $D$  levels. The  $4F$  level may be analyzed in some detail since we were able to determine the variation of  $Q'(4F)$  with pressure down to about 8 mTorr as shown by the data in Fig. 7. The detailed dependence of the  $4F$  apparent cross section on other levels and on the ground-state density may be seen by writing Eq. (27) in the form

$$Q'(4F) = \frac{Q_{ec}(4F) + \bar{c}N \sum_k [Q'(k)/A(k)] Q_t(k \rightarrow 4F)}{1 + [\bar{c}N/A(4F)] \sum_k b(k, 4F) Q_t(k \rightarrow 4F)}, \quad (30)$$

where  $k$  refers to the  $4^1P$  and  $4D$  levels. The apparent cross sections in the above equation are known as a function of pressure and  $Q_t(4D \rightarrow 4F)$  is known from Eq. (28) and the statistical-weight ratio. The unknown quantities of interest are  $Q_t(4^1P \rightarrow 4F)$  and  $Q_{ec}(4F)$ . Because of the rapid decrease with pressure of the transfer terms, we find that at the lower pressures  $Q'(4F)$  is primarily composed of  $Q_{ec}(4F)$  while for larger values of  $N$ ,

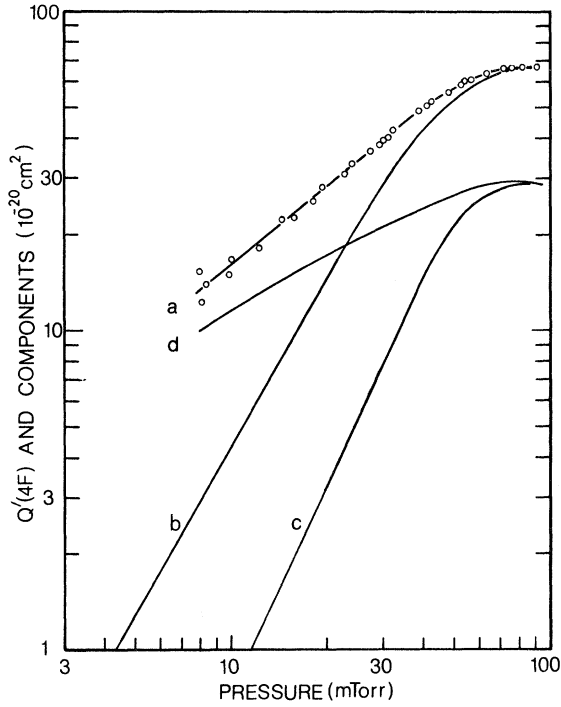


FIG. 7. Contributions to the pressure dependence of the apparent cross section of the  $4F$  level. (a) Apparent cross section of the  $4F$  level. (b) Transfer gain from  $4^1P$  level. (c) Transfer loss to the  $4D$  level. (d) Cascade and electron excitation gain.

$Q'(4F)$  is quite sensitive to the magnitude of  $Q_t(4^1P \rightarrow 4F)$ . We thus use a method of successive approximations to fix the value of  $Q_t(4^1P \rightarrow 4F)$  and to determine values of  $Q_{ec}(4F)$  such that the right-hand side of Eq. (30) shows the best fit to the observed values of  $Q'(4F)$ . The results are shown in Fig. 7 with  $Q_t(4^1P \rightarrow 4F) = (2.5 \pm 0.7) \times 10^{-14} \text{ cm}^2$  and  $Q_{ec}(4F)$  with a value of  $(10 \pm 4) \times 10^{-20} \text{ cm}^2$  at 8 mTorr. It is noteworthy that this value of  $Q_t(4^1P \rightarrow 4F)$  is in excellent agreement with the one deduced in the last section from the  $4^1P$  steady-state equation. The final value is taken as the average and is  $Q_t(4^1P \rightarrow 4F) = (2.3 \pm 0.6) \times 10^{-14} \text{ cm}^2$ . This result is also in excellent agreement with the value  $Q_t(4^1P \rightarrow 4F) = 2 \times 10^{-14} \text{ cm}^2$  determined by Kay and Hughes.<sup>6</sup>

The various contributions to  $Q'(4F)$ , as shown in Fig. 7, appear in the form

$$Q'(4F) = Q_{ec}(4F) + \bar{c}N \sum_k Q_t(j, 4F) \left[ \frac{Q'(k)}{A(k)} - b(k, 4F) \frac{Q'(4F)}{A(4F)} \right], \quad (31)$$

where the brackets indicate the net transfer gain to the  $4F$  level from level  $k$ . The brackets are negative for the  $4D$  level indicating a net loss to this level. This loss is significant only at the higher

pressures and is balanced by input from the  $4^1P$  level and to a lesser extent from  $Q_{ec}(4F)$ . The relatively slow variation of  $Q_{ec}(4F)$  with pressure is reasonable in view of the observed pressure dependence of cascading in other levels, such as  $n^1D \rightarrow 4^1P$ ,  $n^3D \rightarrow 4^3P$ , and  $n^1P \rightarrow 4^1S$ , where the increase with pressure of the low- $n$  cascading levels is partially canceled by the decrease with pressure of the high- $n$  cascading components.

Anderson *et al.*<sup>7</sup> have shown that the  $4F$  cross section does not become pressure independent until pressures somewhat less than 1 mTorr are reached and they have deduced a level cross-section value of  $(1.6 \pm 0.7) \times 10^{-20} \text{ cm}^2$  at 100 eV. Extrapolation of the curve for  $Q'(4F)$  in Fig. 7 shows that the direct electron excitation value of Anderson *et al.* would be approached at a pressure of about 0.5 mTorr.

The preceding analysis of the  $4F$  level indicates that the dominant pressure dependent populating mechanism up to about 20 mTorr is due to  $G$  cascade with direct transfer becoming dominant only at higher pressures. This result confirms earlier work done in this laboratory<sup>27</sup> which indicated that  $Q'(4F)$  at 8 mTorr was much larger than would be expected from direct electron excitation and transfer alone.

#### F. Distribution of Excitation Transfer

The distribution of excitation transfer and cascade gain among various levels at 100 eV and 63 mTorr is given in Table VI. The transfer-gain terms of the  $n^3P$  levels and  $nS$  levels from Table IV are only about 5% of the transfer loss from corresponding  $n^1P$  levels and are not included in Table VI. The net-transfer-gain terms for the  $n^1P$  and  $nD$  levels are obtained from Tables III and V, respectively. Cascade terms are included in parenthesis when such terms are of significant magnitude. The  $4F$  values of transfer gain and

TABLE VI. Distribution of excitation transfer gain  $Q^*(j)$  among various levels at 63 mTorr and 100 eV. Significant cascade terms  $Q_c(j)$  are given in parenthesis. Units are  $10^{-20} \text{ cm}^2$ .

$n j$	$n^1P$	$nD$	$nF$	$\geq nG$
$3^a$	0	0(101)	35(29)	$2 \pm 15$
4	-55	28(24)	20(12)	$13 \pm 8$
5	-47	25(4)	6.2(3)	$10 \pm 5$
6	-33	14(1)	3.2(1)	$9.1 \pm 3.5$
7	-21	7.8	1.2	$6.1 \pm 2.7$
8	-14	3.7	0.9	$5.7 \pm 2.5$
9	-9	2.0	0.5	$29 \pm 12$
10	-7	0.8	0.5	
$> 10^b$	-30	0.5		

<sup>a</sup>Transfer on the  $n=3$  level is not a significant part of the apparent cross sections involved and is zero to within experimental error.

<sup>b</sup>Extrapolated values.

cascade were obtained from Fig. 7. The cascade values for the higher  $F$  levels were estimated by assuming that the decrease in cascade with increasing  $n$  is similar to that observed for the  $D$  levels. Such an assumption only requires that the  $n^{-6}$  decrease in apparent cross section observed for the  $n^1P$ ,  $nD$ , and  $nF$  levels holds also for the  $nG$  levels. Since direct electron excitation contributions to  $Q'(nF)$  appear to be negligible on the basis of  $Q(4F)$  determinations,<sup>7,28</sup> cascade corrections to  $Q'(nF)$  from Table I are sufficient to give  $Q^*(nF)$  for  $n > 4$ .

The net transfer gain summed over all levels of the same  $n$  must be zero for those levels obeying the transfer selection rule  $\Delta n = 0$ . On the  $n = 4$  level the transfer gain found for the  $D$  and  $F$  levels agrees with the independently determined transfer loss from the  $4^1P$  level to within experimental error. Such a situation must also hold up to about  $n = 12$  and may be used to determine the transfer gain for levels with angular momentum  $\geq G$  as shown in Table VI. Although this determination involves considerable error, the fact remains that much of the excitation transfer loss by the higher  $n^1P$  levels does *not* show up as transfer gain in the  $nD$  and  $nF$  levels, and hence considerable excitation transfer must be distributed among levels of angular momentum  $\geq G$ . Because the high orbital angular momentum levels of given  $n$  are practically degenerate in energy, it is likely that further distribution of the transfer-gain terms among  $G$ ,  $H$ , etc., levels is proportional to the statistical weights of these levels.

## V. DISCUSSION

The analysis of the data in the preceding sections gives a more realistic picture of excitation transfer than has been presented in the past. There is little doubt that the primary "reservoir" of excitation energy at high pressure is maintained through the excitation of ground-state atoms to the  $n^1P$  levels by resonance photons. At high values of  $n$ , much of this energy is transferred to states of higher orbital angular momentum by collisions with ground-state atoms, the net transfer following  $\Delta L = 1, 2$ , and possibly  $\Delta L = 3$  with  $\Delta n = 0$  for  $n \leq 12$ . This energy input must be balanced by radiative emission through cascade processes, which are more probable to the smaller values of  $n$  and  $L$ , and are primarily  $\Delta L = -1$  transitions with  $\Delta n \neq 0$ . It is particularly noteworthy that because of the relatively large amount of transfer input to levels with  $nL \geq nG$  we may expect that cascading such as  $nH \rightarrow 5G$  and  $nG \rightarrow 4F$  plays a significant part in populating these terminal  $L$  levels. Such large cascading is indeed observed to occur for other terminal  $L$  levels, i. e.,  $nF \rightarrow 3D$ ,  $nD \rightarrow 2P$ , and  $nP \rightarrow 1S$ .

The cross sections for excitation transfer be-

tween the  $4^1P$  and  $4F$  and between the  $4D$  and  $4F$  levels were found to be of the same order of magnitude. This is reasonable since the stronger selection rule  $\Delta L = \pm 2$  is offset somewhat by the larger energy difference between the  $4^1P$  and  $4F$  levels. On the other hand, the  $4D$  and  $4F$  levels are considerably closer in energy but the transfer interaction is of the  $L = \pm 1$  type.

Other workers have attempted to explain the pressure dependence of the  $D$  levels by observing relatively few of the  $P$  and  $D$  levels and by introducing various assumptions or models concerning the transfer processes involved. Lees and Skinner<sup>1</sup> and Maurer and Wolf<sup>2</sup> concluded that the transfer was of the  $\Delta L = \pm 1$  type such as  $n^1P \rightarrow n^{1,3}D$ . Their conclusions violate the Wigner spin rule, do not consider other  $\Delta L$  interactions, and do not consider the effect of large cascade populations. They did, however, show that electron-ion recombination excitation was unimportant.

Gabriel and Heddle<sup>3</sup> showed that cascading was an important process in populating  $D$  levels but assumed that only  $\Delta L = 0, 1$  transfer was important and further assumed that the spin rule was only weakly obeyed for near resonance conditions.

St. John and Fowler<sup>4</sup> introduced a model whereby only  $\Delta L = \pm 2$  transfer was considered and the high populations of the  $D$  states were caused by  $n^1P \rightarrow nF$  transfer followed by  $nF \rightarrow mD$  cascading where  $m < n$ . This model avoided the difficulties caused by spin rule violations since the  $nF$  levels have only weak Russell-Saunders coupling. Our present work shows that this model apparently holds for the  $3D$  level in that all excess population of this level may be accounted for by cascading. This does not prove, however, that an  $nF$  level is subject only to the transfer interaction  $\Delta L = 2$  with a  $n^1P$  level. The model also breaks down for the higher  $nD$  levels as direct collisional population becomes more significant than cascading into these levels.

The excess population in the upper  $D$  and  $F$  states and the deficiency in the  $^1P$  states might seem to be due in part to processes other than direct transfer processes. Some collision process might form molecules, atomic ions, or molecular ions from the  $^1P$  species and a second collision or transition could add to the population of the  $D$  and  $F$  states. In general, these processes would populate the low lying  $D$  states much more than the upper  $D$  states. The energy dependence of  $Q'(nD)$  at high pressure, while similar to the  $n^1P$  states, is also similar in shape to the ionization cross-section curve for helium. Calculations were made for radiative recombination of positive ions and electrons to determine the possible effects of this process. Hydrogenic recombination coefficients calculated by Burgess<sup>29</sup> were used in determining the electron density necessary to account for  $Q^*(5D)$  by recom-

bination. This density, and the accompanying larger coefficient for recombination into the 3D level predict  $Q^*(3D)$  to be  $65 \times 10^{-20} \text{ cm}^2$  contrary to the measured value of about zero. All excess 3D population is accounted for by measured cascade from F levels. Another consideration mitigating against volume recombination processes is that the apparent cross sections are observed to be independent of electron current at all pressures. Wall recombination would become important at some

pressure and cause  $Q'(j)$  to be nonlinear with respect to  $I$ . These findings are in agreement with the early work of Maurer and Wolf.<sup>2</sup>

#### ACKNOWLEDGMENTS

Acknowledgment is due Dr. J. D. Walker, Jr., for his work with liquid-nitrogen-cooled lead-sulfide detectors in the acquisition of the data on the radiation from the F states.

\*Research supported in part by the Air Force Office of Scientific Research, Office of Aerospace Research, USAF under Grant No. AF-AFOSR-252-67.

†Present address: Shell Oil Co., Houston Research Laboratory, Deer Park, Tex. 77536.

<sup>1</sup>J. H. Lees and H. W. B. Skinner, Proc. Roy. Soc. (London) A137, 186 (1932).

<sup>2</sup>W. Maurer and R. Wolf, Z. Physik 115, 410 (1940).

<sup>3</sup>A. H. Gabriel and D. W. O. Heddle, Proc. Roy. Soc. (London) A258, 124 (1960).

<sup>4</sup>R. M. St. John and R. G. Fowler, Ann. Phys. (N.Y.) 15, 461 (1961).

<sup>5</sup>R. M. St. John and T. W. Nee, J. Opt. Soc. Am. 55, 426 (1965).

<sup>6</sup>R. B. Kay and R. H. Hughes, Phys. Rev. 154, 61 (1967).

<sup>7</sup>R. J. Anderson, R. H. Hughes, and T. G. Norton, Phys. Rev. 181, 198 (1969).

<sup>8</sup>R. L. Abrams and G. J. Wolga, Phys. Rev. Letters 19, 1411 (1967).

<sup>9</sup>D. R. Bates, Discussions Faraday Soc. 33, 7 (1962).

<sup>10</sup>E. C. G. Stueckelberg, Helv. Phys. Acta 5, 370 (1932).

<sup>11</sup>N. F. Mott and H. S. W. Massey, *The Theory of Atomic Collisions*, 3rd ed. (Oxford U.P., London, 1965), p. 654.

<sup>12</sup>C. C. Lin and R. G. Fowler, Ann. Phys. (N.Y.) 15, 461 (1961).

<sup>13</sup>F. T. Chan, Phys. Rev. 172, 96 (1968).

<sup>14</sup>E. Wigner, Nachr. Ges. Wiss. Göttingen 375 (1927).

<sup>15</sup>J. D. Jobe and R. M. St. John, Phys. Rev. 164, 117 (1967).

<sup>16</sup>R. M. St. John, C. C. Lin, R. L. Stanton, H. D. West, J. P. Sweeny, and E. A. Rinehart, Rev. Sci. Instr. 33, 1089 (1962).

<sup>17</sup>R. M. St. John, *Methods of Experimental Physics* (Academic, New York, 1969), Vol. 8, p. 27.

<sup>18</sup>J. C. De Vos, Physica 20, 690 (1954).

<sup>19</sup>General Electric Co., standard lamp type 30AT24/13.

<sup>20</sup>W. L. Wiese, M. W. Smith, and B. M. Glennon, Natl. Std. Ref. Data Ser., Natl. Bur. Std. (U.S.) NSRDS-NBS 4 (1966).

<sup>21</sup>F. E. Niles, U. S. Army Ballistic Research Laboratories, Aberdeen Proving Ground, Aberdeen, Md., Report No. 1354, 1967 (unpublished).

<sup>22</sup>E. U. Condon and G. H. Shortley, *The Theory of Atomic Spectra* (Cambridge U.P., London, 1951), p. 131.

<sup>23</sup>A. V. Phelps, Phys. Rev. 110, 1362 (1958).

<sup>24</sup>Y. K. Kim and M. Inokuti, Phys. Rev. 175, 176 (1968).

<sup>25</sup>Y. K. Kim and M. Inokuti, Phys. Rev. 184, 38 (1969).

<sup>26</sup>B. L. Moiseiwitsch and S. J. Smith, Rev. Mod. Phys. 40, 238 (1968).

<sup>27</sup>J. D. Jobe and R. M. St. John, J. Opt. Soc. Am. 57, 1449 (1967).

<sup>28</sup>S. Chung and C. C. Lin, Bull. Am. Phys. Soc. 13, 214 (1968).

<sup>29</sup>A. Burgess, Monthly Notices Roy. Astron. Soc. 69, 1 (1964).